The land-surface scheme of the Rossby Centre regional atmospheric climate model (RCA3)

Patrick Samuelsson, Stefan Gollvik, Anders Ullerstig
Rossby Centre

The land-surface scheme of the Rossby Centre regional atmospheric climate model (RCA3)

Patrick Samuelsson, Stefan Gollvik, Anders Ullerstig
Rossby Centre

Report Summary / Rapportsammanfattning

Issuing Agency/Utgivare	Report number/Publikation
Swedish Meteorological and Hydrological Institute S-601 76 NORRKÖPING Sweden	Meteorologi nr 122
	Report date/Utgivningsdatum
	December 2006

Author (s)/Författare

Patrick Samuelsson, Stefan Gollvik and Anders Ullerstig

Title (and Subtitle/Titel

The land-surface scheme of the Rossby Centre regional atmospheric climate model (RCA3)

Abstract/Sammandrag

This report describes the physical processes as part of the Land-Surface Scheme (LSS) in the Rossby Centre Regional Atmospheric Climate Model (RCA3). The LSS is a tiled scheme with the three main tiles with respect to temperature: forest, open land, and snow. The open land tile is divided into a vegetated and a bare soil part for latent heat flux calculations. The individual fluxes of heat and momentum from these tiles are weighted in order to obtain grid-averaged values at the lowest atmospheric model level according to the fractional areas of the tiles. The forest tile is internally divided into three sub-tiles: forest canopy, forest floor soil, and snow on forest floor. All together this gives three to five different surface energy balances depending on if snow is present or not.

The soil is divided into five layers with respect to temperature, with a no-flux boundary condition at three meters depth, and into two layers with respect to soil moisture, with a maximum depth of just above 2.2 meters. Runoff generated at the bottom of the deep soil layer may be used as input to a routing scheme.

In addition to the soil moisture storages there are six more water storages in the LSS: interception of water on open land vegetation and on forest canopy, snow water equivalent of open land and forest snow, and liquid water content in both snow storages.

Diagnostic variables of temperature and humidity at 2m and wind at 10m are calculated individually for each tile.

Key words/sök-, nyckelord

Land-Surface Scheme, Regional climate model

Supplementary notes/Tillägg	Number of pages/Antal sidor	Language/Språk
	25	English

ISSN and title/ISSN och title

0283-7730 SMHI Meteorologi

Report available from/Rapporten kan köpas från:

SMHI
SE-601 76 NORRKÖPING
Sweden

Contents

1 Introduction

Coupled numerical simulations over several decades are needed in order to better understand present and future climate variability. The term *coupled* refers to atmospheric, land surface and oceanic processes. For long simulations it is important that the energy and water cycles are in balance. If any cycle is out of balance some flux corrections must be applied. In the case of regional modelling, the model used as boundary condition will also keep the simulation on track.

Questions that the results from climate simulations aim to answer vary in both space and time. For example, farmers may want to know if the diurnal temperature range will change during the spring season in a specific region or the hydro-power industry might want to know if the annual water supply to their dams will change with time. Thus, the model systems should be able to resolve various processes on time scales ranging from hours to years.

Simulating variability on a short time scale (sub daily) involves fast-response processes. This means that complex feedback mechanisms involved must be more realistically described in the model than is needed to capture only slower variability.

The aim of the present paper is to present a land-surface scheme (LSS) which has the ability to resolve processes ranging from hourly to annually. The LSS has been developed with focus on physical processes which involve snow and frozen soil at mid and high latitudes. The main purposes of the scheme are: (i) to act as a lower boundary condition for the atmosphere. This means providing the atmosphere with realistic radiation, heat, and momentum fluxes, (ii) to provide the ocean with realistic runoff and (iii) to realistically simulate some key land-surface diagnostics like 2 meter temperature and humidity, 10 meter wind speed, and snow extent.

The LSS is part of the Rossby Centre Regional Atmospheric Climate Model (RCA3). For an evaluation of RCA3 please refer to Kjellström et al. (2006).

2 General LSS setup

The present scheme is a so-called tiled scheme which means that individual sub surfaces or tiles within a grid square are characterised with unique values of surface properties like type of vegetation, roughness length and albedo. A separate energy balance is also calculated for each tile. Different tiles respond differently to changes in fluxes depending on their heat capacity and heat transfer characteristics. Typical fast-response tiles are forest and snow surfaces. Forests have low heat capacity while snow has low heat transfer capacity. Thus, the temperature of these surfaces is quickly reflected in the grid-averaged two meter temperature. Slower temperature changes depend largely on phase changes and the heat capacity of the whole soil column. In this case the amount of snow storage and soil freezing processes are important.

Another approach in land surface modelling, which nowadays is being replaced by the tile approach, is the parameter averaging (mixture) approach. In the pure parameter averaging approach, all sub-surface properties of a grid square are averaged together so that only one value per grid square is used for each individual surface property. Here, only one energy balance is used to represent the whole grid square. Generally the tile approach gives a better representation of the physical processes than the parameter averaging approach. However, for a very small scale, heterogeneous landscape and/or during very windy conditions the parameter averaging approach will probably reflect the physical processes more realistically (Koster and Suarez, 1992).
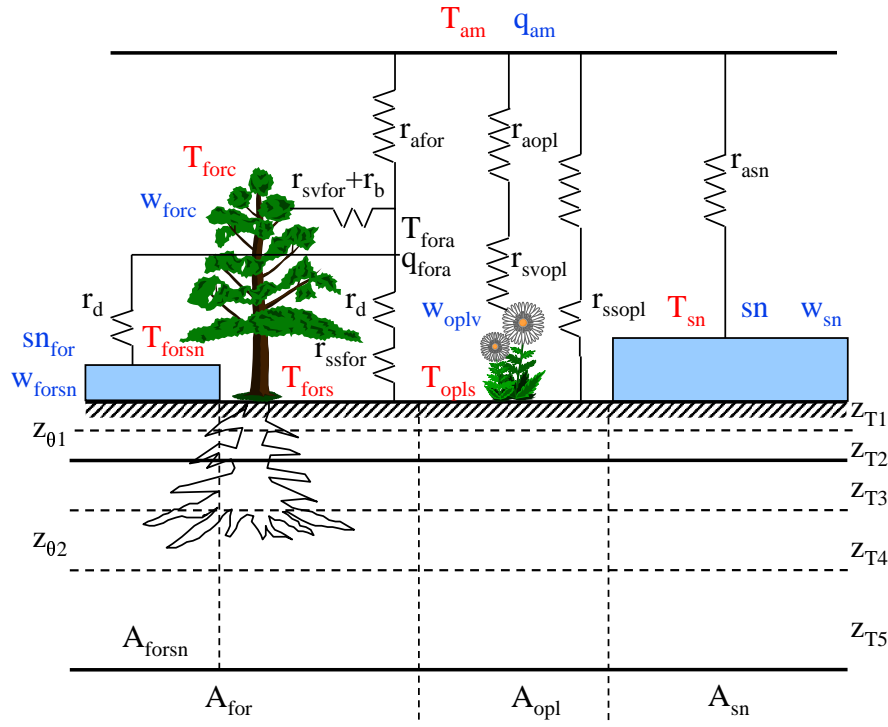
Figure 1: A principal sketch of the land-surface scheme in RCA3. The LSS is divided into three main tiles: forest (A_{for}), open land (A_{opl}) and snow on open land (A_{sn}). The forest also has a snow sub-tile (A_{forsn}). Prognostic temperatures are marked in red while the water prognostic variables are marked in blue. Each individual tile is connected to the lowest atmospheric level via their corresponding aerodynamic resistances (r_a). For evapotranspiration calculations a number of surfaces resistances are used (r_s).

Parameter	Definition	Reference	Parameter	Definition	Reference
Sub-grid fractions			**Resistances**		
A_{for}	fractional area of forest		r_{svfor}	forest canopy surface resistance	Eq 10
A_{opl}	fractional area of open land		r_{svopl}	open land vegetation surface resistance	Eq 10
A_{sn}	fractional area of open-land snow	Sec 3.7.1	r_{ssfor}	forest floor soil surface resistance	Eq 19
A_{forsn}	fractional area of snow in forest	Sec 3.7.1	r_{ssopl}	open land soil surface resistance	Eq 19
Prognostic temperatures			r_{afor}	aerodynamic resistance above forest	Sec 3.1
T_{opls}	open land soil surface temperature		r_{aopl}	aerodynamic resistance above open land	Sec 3.1
T_{sn}	snow surface temperature	Eq 32	r_{asn}	aerodynamic resistance above snow	Sec 3.1
T_{sns}	soil temperature below snow		r_b	aerodynamic resistance (forest canopy - canopy air)	Eq 46
T_{forsn}	forest snow surface temperature	Eq 24			
T_{fors}	forest soil surface temperature	Eq 24	r_d	aerodynamic resistance (forest floor - canopy air)	Eq 48
T_{forsns}	soil temperature below forest snow				
T_{forc}	forest canopy temperature	Eq 24	**Depth of soil layers**		
Prognostic water storages			$z_{T1}-z_{T5}$	thickness of soil layers w.r.t. temperature (0.01, 0.062, 0.21, 0.72, 1.89 m)	
sn	open land snow water equivalent	Sec 3.7	$z_{\theta1}-z_{\theta2}$	thickness of soil layers w.r.t. soil moisture (0.072, 2.2 m (1.0 m in mountainous areas))	
sn_{for}	forest snow water equivalent	Sec 3.7			
w_{oplv}	intercepted water on low vegetation	Sec 3.2	**Albedo and emissivity (value/prognostic)**		
w_{forc}	intercepted water on forest canopy	Sec 3.2	α_{opls}	open land surface albedo (0.28)	
w_{sn}	snow liquid water	Sec 3.7	α_{forc}	forest canopy albedo (0.15)	
w_{forsn}	forest snow liquid water	Sec 3.7	α_{fors}	forest soil surface albedo (0.15)	
			α_{forsn}	forest snow surface albedo (0.2)	
			α_{sn}	snow surface albedo (prognostic)	Sec B.2
			ε_{opls}	open land surface emissivity (0.985)	
			ε_{forc}	forest canopy emissivity (0.985)	
			ε_{fors}	forest soil surface emissivity (0.985)	
			ε_{forsn}	forest snow surface emissivity (0.99)	
			ε_{sn}	snow surface emissivity (0.99)	
			ε_{desert}	desert surface emissivity (0.93)	

From an atmospheric point of view, the present LSS, as shown in Figure 1, has three tiles with respect to temperature: forest, open land, and snow. The open land tile is divided into a vegetated and a bare soil part for latent heat flux calculations. The individual fluxes of heat and momentum from these tiles are weighted in order to obtain grid-averaged values at the lowest atmospheric model level according to the fractional areas of the tiles. Local surface layer equilibrium is assumed for each tile which means that they have their own aerodynamic resistances. The forest tile is internally divided into three sub-tiles: forest canopy, forest floor soil, and snow on forest floor. The motivation for this division comes from the fact that these sub-tiles are closely related to each other with regards to their temperature and humidity conditions in the canopy air space. All together this gives three to five different surface energy balances depending on if snow is present or not.

The soil is divided into five layers with respect to temperature and consists of two to four sub-tiles depending on if snow is present or not. The discretization of the soil generally follows that of Viterbo and Beljaars (1995) except for the two top-most soil layers which are 1.0 and 6.2 cm, respectively. At the bottom we use a no-flux boundary condition.

There are eight prognostic water storages in the LSS: interception of water on open land vegetation and on forest canopy, snow water equivalent of open land and forest snow, liquid water content in both snow storages, and two soil moisture storages. Interception of snow is not included.

The soil moisture is assumed to be independent on surface coverage which gives only two prognostic soil moisture storages: top and deep soil moisture. The top soil moisture layer has a depth corresponding to the depth of the two top-most soil layers for temperature while the depth of the deep layer is 1.0 m in mountainous areas and 2.2 m outside mountainous areas. Runoff from the deep layer may be used as input to a routing scheme.

Diagnostic variables of temperature and humidity at 2m and wind at 10m are calculated using Monin-Obukhov similarity theory as described in Appendix C. These diagnostic variables are calculated individually for each tile and are then area-averaged for larger sub-surfaces or for whole grid squares.

3   Specific LSS processes

Here, the individual processes as part of the LSS will be described separately. But, all these processes are tightly connected to each other. To illustrate this we take the 2m-temperature, representing one of the most important diagnostics produced by a LSS, as a starting point in the chain of dependencies between the LSS processes. The 2m-temperature is a result of complicated feedback mechanisms between the surface and the atmospheric surface layer. It is strongly connected to the prognostic surface temperatures which are closely related to the fluxes of sensible and latent heat. An underestimation of, for example, latent heat flux would produce a positive bias in sensible heat flux in order to fulfill the energy balance, which implies a positive bias in the surface temperature. The problem is that there could be many reasons for a wrong latent heat flux; the aerodynamic resistance could be wrong due to incorrect roughness lengths or errors in the estimations of turbulence intensity, and in the case of vegetation, errors in leaf area index (LAI), soil moisture content and surface resistance can all affect the transpiration. The heat capacity of the surface elements (canopy, snow, soil surface) is important for the diurnal surface temperature variations which will affect surface saturation humidity and therefore also the latent heat flux. These processes are certainly important for the diurnal variations in 2m temperature but any errors will, of course, also affect the seasonal and annual mean temperatures.

To correctly describe seasonal and annual variations in 2m temperature, the LSS must also include

processes related to snow cover and soil freezing. Snow is an extreme in many respects. It has high albedo which reduces available net radiation. It stores frozen water at the surface which requires a lot of energy to melt, and it has low heat transfer capability which more or less isolates the soil from the atmosphere. Thus, it is very important to catch the areal and temporal extent of snow, not only for simulating temperature, but also for river flows affected by snow melt. Soil freezing needs to be accounted for since it acts to delay temperature drop in autumn and temperature rise in spring.

3.1 Heat fluxes and aerodynamic resistance

The sensible (H) and latent (E) heat fluxes between the surface and the first atmospheric level at height z_{am} ($\sim$90 m in the present RCA3 set-up with 24 vertical levels) are parameterized as

$$H = \rho c_p \frac{T_s - T_{am}}{r_a} \tag{1}$$

and

$$E = \rho L_e \frac{q_s(T_s) - q_{am}}{r_a + r_s}. \tag{2}$$

Here, ρ is air density, c_p is heat capacity of the air, L_e is latent heat of vaporisation of water, T_s is surface temperature, T_{am} is temperature at z_{am}, q_s is surface saturated specific humidity, q_{am} is specific humidity at z_{am} and r_a aerodynamic resistance. The formulation of the surface resistance r_s depends on the surface as described in Section 3.3.

The aerodynamic resistance is important for both fast response processes such as diurnal temperature range and for long term performance such as a correct division of precipitation into evapotranspiration and runoff. The LSS has three different aerodynamic resistances represented by the characteristics of forest, open land, and snow, with respect to surface temperature and roughness lengths of momentum and heat. The aerodynamic resistance for heat is given by the drag coefficient, C_h:

$$C_h = \frac{1}{u r_a} = \frac{k^2}{\ln(z_{am}/z_{0m}) \ln(z_{am}/z_{0h})} f_h(Ri, z_{am}/z_{0h}), \tag{3}$$

where u is wind speed at z_{am}, k is the von Karman's constant, z_{0m} and z_{0h} are roughness lengths for momentum and heat, respectively, Ri is the Bulk-Richardson number and f_h represents analytic stability functions based on modified Louis et al. (1981) formulations.

The dependence of the heat fluxes on the aerodynamic resistance is strong. This in turn has been shown to be quite sensitive to the ratio between the roughness length of heat and momentum (Beljaars and Viterbo, 1994; Chen et al., 1997; Samuelsson et al., 2003; van den Hurk and Viterbo, 2003). However, the problem is that estimations of the ratio z_{0m}/z_{0h} vary considerably. According to Chen et al. (1997) it is reasonable to relate the ratio to the properties of the flow as suggested by Zilitinkevich (1995):

$$\frac{z_{0m}}{z_{0h}} = \exp(kC\sqrt{Re^*}), \tag{4}$$

where

$$Re^* = \frac{u_0^* z_{0m}}{\nu}, \tag{5}$$

where ν is the kinematic molecular viscosity, Re^* is the roughness Reynolds number, and u_0^* is the surface friction velocity. C is an empirical constant which Chen et al. (1997) estimated to be 0.1 based on comparisons between simulations and observations of heat fluxes. r_a is sensitive to the value of C for large values on z_{0m} (> 0.2 m) and to the value of z_{0m} for small values on z_{0m} (< 0.1 m). The presently relatively thick (90 m) lowest atmospheric layer in RCA allows a long time step of 30 minutes, but to maintain a reasonably high surface heat flux we have been forced to assume $z_{0h} = z_{0m} = 0.2$ m for snow free open land. Thus the Zilitinkevich formulation of the ratio z_{0m}/z_{0h} is used only for snow surfaces with $z_{0m} = 0.002$ m. For forest we use $z_{0h} = z_{0m}$ as suggested by Mölder and Lindroth (1999), which also gives good results when comparing simulated and observed heat fluxes. z_{0m} for forest is a seasonally dependent value in the range 0.81–1.06 m.

3.2 Interception of rain on vegetation

Rain intercepted by the vegetation is available for potential evaporation which means that it has a strong influence on the fluxes of heat and consequently also on the surface temperature. So far interception of snow is not included in the present LSS. A version exists where it is implemented and it will be part the official LSS after further testing. Thus, at present we have only a prognostic storage of liquid water on the vegetation. Below freezing ($T_{forc} \leq 0°C$) rain is intercepted. Any water present will stay on the vegetation and evaporate as super-cooled water. The parameterization of interception of rain follows Noilhan and Planton (1989) and its implementation into RCA3 is similar to the implementation in RCA2 as described by Bringfelt et al. (2001). The rate of change of intercepted water is described by

$$\frac{w_{veg}^{\tau+1} - w_{veg}^{\tau}}{\Delta t} = \text{veg}(P - \frac{\delta}{L_e} E_v), \tag{6}$$

where w_{veg} is amount of intercepted water (mm of water on the specified fraction), τ and $\tau + 1$ represent present and next time step, Δt is the length of the time step (s), veg is a vegetation cover parameter, P is rain intensity (kg m^{-2} s^{-1}), E_v is evaporation of intercepted water (W m^{-2}), and δ is the fraction of of the vegetation covered with water defined as (Deardorff, 1978)

$$\delta = \left(\frac{w_{veg}}{w_{vegmax}} \right)^{2/3}. \tag{7}$$

The exponent 2/3 comes from the fact that the intercepted water exists in the form of droplets where the water volume of the droplets is proportional to r^3, where r is the radius of the droplets, and the surface of the droplets is proportional to r^2. $w_{vegmax} = 0.2 \cdot \text{veg} \cdot \text{LAI}$ is the maximum amount of water allowed on the vegetation (Dickinson, 1984). Here LAI is the leaf area index as defined in Section 3.3.

The evaporation E_v is calculated according to

$$E_v = \rho L_e \frac{q_s(T_s) - q_{am}}{r_a}. \tag{8}$$

6

To keep the solution numerically stable δ is solved implicitly

$$\delta = (1-\alpha)\left(\frac{w_{veg}^{\tau}}{w_{vegmax}}\right)^{2/3} + \alpha\left(\frac{w_{veg}^{\tau+1}}{w_{vegmax}}\right)^{2/3}, \tag{9}$$

where α represents the degree of implicitly (set to 0.5). $w_{veg}^{\tau+1}$ is found by replacing δ in Equation 6 with Equation 9. The resulting equation is solved using the Newton-Raphson's method.

The new value of intercepted water amount may not exceed the maximum value. Thus, any excess water becomes throughfall, $thr = \max(0.0, (w_{veg}^{\tau+1} - w_{vegmax})/\Delta t)$. The final water amount is corrected with the throughfall as $w_{veg}^{\tau+1} = w_{veg}^{\tau+1} - thr \cdot \Delta t$ and the total amount of rain that falls to the ground becomes $P_{tot} = thr + (1.0 - \text{veg})P$.

This parameterization is used for interception of rain on both forest canopy and on open land vegetation with individual values for the parameters veg and LAI. In the forest case $T_s = T_{forc}$, $q_{am} = q_{fora}$, and $r_a = r_b$ and in the open land case $T_s = T_{opls}$ and $r_a = r_{aopl}$.

3.3   Surface resistances

For latent heat flux a surface resistance is added for vegetation transpiration and for bare soil evaporation. Snow surfaces and intercepted water have zero surface resistance. In the case of condensation, $q_s(T_s) < q_{am}$, the surface resistance is also put to zero.

The vegetation surface resistance, closely following Noilhan and Planton (1989), is a function of a vegetation dependent minimum surface resistance, r_{svmin}, the LAI, and five factors representing (F_1) the influence of photosynthetically active radiation, (F_2) the effect of water stress, (F_3) the effect of vapor pressure deficit, (F_4) an air temperature dependence, and (F_5) a soil temperature dependence:

$$r_{sv} = \frac{r_{svmin}}{\text{LAI}} F_1 F_2^{-1} F_3^{-1} F_4^{-1} F_5^{-1}. \tag{10}$$

The photosynthetically active radiation is assumed to be $0.55 S{\downarrow}$, where $S{\downarrow}$ is the incoming shortwave radiation. The factor F_1 is defined as

$$F_1 = \frac{1+f}{f + r_{svmin}/r_{svmax}}, \tag{11}$$

with

$$f = 0.55 \frac{S{\downarrow}}{S_L} \frac{2}{\text{LAI}}, \tag{12}$$

where r_{svmax} is a maximum surface resistance set to 5000 s m^{-1} and S_L is a limit value of 30 W m^{-2} for a forest and of 100 W m^{-2} for a crop.

The factor F_2 varies between 0 and 1 depending on available soil moisture θ:

$$F_2 = \begin{cases} 1, & \text{if } \theta > \theta_{cr} \\ \dfrac{\theta - \theta_{wi}}{\theta_{cr} - \theta_{wi}}, & \text{if } \theta_{wi} \leq \theta \leq \theta_{cr} \\ 0, & \text{if } \theta < \theta_{wi} \end{cases} \tag{13}$$

where θ_{wi} is the wilting point, $\theta_{cr} = 0.9\theta_{fc}$ and θ_{fc} is the field capacity. To account for different soil moisture conditions in different root layers the factor F_2 is calculated individually for each soil layer which in combination with the other factors actually gives different r_{sv}-values for each soil layer. These r_{sv}-values are finally weighted with respect to the depth of each soil layer.

Factor F_3 represents the effect of vapor pressure deficit of the atmosphere or, as expressed here, in terms of specific humidity (Jarvis, 1976; Sellers et al., 1986):

$$F_3 = 1 - g(q_s(T_s) - q_{am}), \tag{14}$$

where g is a vegetation-dependent empirical parameter set to 0.04 for a forest and to zero for a crop. In the forest case $T_s = T_{forc}$ and $q_{am} = q_{fora}$ and in the open land case $T_s = T_{opls}$.

The air temperature has a strong influence on the transpiration with the most favorable conditions at 25°C. The factor F_4 describes the air temperature dependence following Dickinson (1984)

$$F_4 = 1.0 - 0.0016(298.0 - T_{am})^2, \tag{15}$$

where $T_{am} = T_{fora}$ in the forest case.

The vegetation does not become active in spring until the soil temperature in the root zone reaches at least +2°C. Therefore, an additional factor, $F_5 = 1 - f(T)$, is added which varies between 0 and 1 for soil temperatures between $T_1 = T_{melt} + 4$ K and $T_2 = T_{melt} + 2$ K following a sinusoidal function originally intended for parameterization of soil freezing as described in Viterbo et al. (1999):

$$f(T) = \begin{cases} 0, & T > T_1 \\ 0.5\left[1 - \sin\left(\dfrac{\pi(T - 0.5T_1 - 0.5T_2)}{T_1 - T_2}\right)\right], & T_2 \leq T \leq T_1 \\ 1, & T < T_2. \end{cases} \tag{16}$$

As for F_2, this gives different F_5-values for different soil layers depending on their temperature.

There are separate leaf area indexes (LAI) for open land vegetation, for coniferous forest and for deciduous forest. The coniferous forest LAI, LAI_{cf}, is set constant to 4.0 while the open land vegetation and deciduous forest LAIs are parameterised as functions of soil temperature (Hagemann et al., 1999):

$$\text{LAI}_T = \text{LAI}_{min} + f(T_{soil})(\text{LAI}_{max} - \text{LAI}_{min}), \tag{17}$$

where

$$f(T_{soil}) = 1 - \left(\frac{T_{max} - T_{soil}}{T_{max} - T_{min}}\right)^2. \tag{18}$$

8

The allowed range in LAI, defined by the maximum and minimum values LAI_{max} and LAI_{min}, are set to 0.4–2.3 for open land vegetation and to 0.4–4.0 for deciduous forest, respectively. LAI does not show sub-diurnal variability. Thus, the soil temperature, T_{soil}, in Equation 18 has to be unaffected by diurnal variations why we have chosen the temperature in the fourth soil layer. The minimum and maximum temperatures, T_{min} and T_{max}, are set to 273.0 and 293.0 K, respectively. All LAI values are set to LAI_{min} for soil moisture values $\theta_s \leq \theta_{wi}$, where θ_{wi} is the wilting point.

Bare soil evaporation is restricted by the soil surface resistance (van den Hurk et al., 2000):

$$r_{ss} = \frac{r_{ssmin}}{1 - f(T)} \frac{\theta - \theta_{wi}}{\theta_{fc} - \theta_{wi}},$$ (19)

where r_{ssmin} represents a minimum value of the surface resistance ($= 50$ sm^{-1}). As described in Section 3.8 there is no solid phase of soil water, therefore, $1 - f(T)$ is used to represent the fraction of liquid soil water to total soil water in the top soil layer with $T_1 = T_{melt} + 1$ K and $T_2 = T_{melt} - 3$ K.

3.4 Evapotranspiration

In the case of wet vegetation the total evapotranspiration is the sum of evaporation of intercepted water, E_v in Equation 8, and transpiration via stomata, as expressed through Equation 2. The total evapotranspiration, E_c, is defined as

$$E_c = \rho L_e h_v \frac{q_s(T_s) - q_{am}}{r_a + r_{sv}},$$ (20)

where the Halstead coefficient, h_v, includes the fraction of the vegetation covered with water, δ,

$$h_v = h_v^{tr} + h_v^{int} = (1 - k\delta) + \frac{r_a + r_{sv}}{r_a} k\delta.$$ (21)

The coefficient is subdivided into a transpiration part, h_v^{tr}, and into an interception part, h_v^{int}. The Halstead coefficient, as defined in Noilhan and Planton (1989), is modified by introducing the factor k to take into account the fact that also saturated vegetation can transpire, i.e. when $\delta = 1$ (Bringfelt et al., 2001). k=0 would represent a situation where the intercepted water forms full spheres just touching the vegetation surface and therefore allow full transpiration from the whole leaf surface. k=1 would represent a situation where a water film covers the vegetation completely and no transpiration is allowed. To adhere the interception model as described above, where the intercepted water exists as droplets, we set the value of k to 0.25. Note that in the case of condensation, i.e. $E_c < 0$, $h_v = (r_a + r_{sv})/r_a$.

3.5 Forest processes

The forest canopy is characterized by low heat capacity which means that its temperature responds fast to changes in fluxes. Thus, to realistically simulate diurnal variations in 2m-temperature in a forest dominated landscape this effect must be accounted for. The forest canopy acts more or less like a cover above the forest floor, therefore, it is really the temperature and specific humidity conditions in the canopy air space, T_{fora} and q_{fora}, that set the conditions for heat fluxes between forest canopy,

9

forest floor, and lowest model level in the forest tile. T_{fora} and q_{fora} are diagnostic variables which have to be solved iteratively as described in Appendix D. The heat fluxes are expressed as:

	Sensible heat flux	**Latent heat flux**
Forest canopy	$H_{forc} = \rho c_p \dfrac{T_{forc} - T_{fora}}{r_b}$	$E_{forc} = \rho L_e h_{vfor} \dfrac{q_s(T_{forc}) - q_{fora}}{r_b + r_{svfor}}$
Forest floor (soil)	$H_{fors} = \rho c_p \dfrac{T_{fors} - T_{fora}}{r_d}$	$E_{fors} = \rho L_e \dfrac{q_s(T_{fors}) - q_{fora}}{r_d + r_{ssfor}}$
Forest floor (snow)	$H_{forsn} = \rho c_p \dfrac{T_{forsn} - T_{fora}}{r_d}$	$E_{forsn} = \rho L_e \dfrac{q_s(T_{forsn}) - q_{fora}}{r_d}$
Canopy air - Atmos.	$H_{for} = \rho c_p \dfrac{T_{fora} - T_{am}}{r_{afor}}$	$E_{for} = \rho L_e \dfrac{q_s(T_{fora}) - q_{am}}{r_{afor}}$

$$(22)$$

Here r_b and r_d are the aerodynamic resistances between the forest canopy and the canopy air and between the forest floor and the canopy air, respectively. The Halstead coefficient, h_{vfor}, is defined by replacing r_a with r_b, r_{sv} with r_{svfor}, and δ with δ_{forc} in Equation 21, respectively.

The bulk aerodynamic resistance r_b and the aerodynamic resistance r_d, defined in Appendix A, are both based on Choudhury and Monteith (1988).

Since each sub surface within the forest tile has its own energy balance the net radiation components must be separated between the forest canopy and the forest floor according to

$$
\begin{cases}
Rn_{forc} = & (1-\chi)(1-\alpha_{forc})S\downarrow + (1-\chi)\varepsilon_{forc}\{L\downarrow + \sigma[(1-A_{forsn})T_{fors}^4 + \\
& A_{forsn}T_{forsn}^4 - 2T_{forc}^4]\} \\
Rn_{fors} = & \chi(1-\alpha_{fors})S\downarrow + \varepsilon_{fors}\{\chi L\downarrow + \sigma[(1-\chi)T_{forc}^4 - T_{fors}^4]\} \\
Rn_{forsn} = & \chi(1-\alpha_{forsn})S\downarrow + \varepsilon_{forsn}\{\chi L\downarrow + \sigma[(1-\chi)T_{forc}^4 - T_{forsn}^4]\}
\end{cases}
\tag{23}
$$

where $L\downarrow$ is incoming longwave radiation and α and ε are albedo and emissivity values, respectively, as specified in Figure 1. In the separation a sky view factor, $\chi = \exp(-0.5 \cdot \text{LAI})$, is used which describes the degree of canopy closure and is defined as the fraction of sky that the ground under the canopy sees (Verseghy et al., 1993). This definition is strictly valid only for longwave radiation in combination with needle-leaf trees. However, we apply it more generally, i.e., for all forest types and for both short- and longwave radiation.

The total flux at the surface is defined as $\phi_{forx} = Rn_{forx} + H_{forx} + E_{forx}$, where x is one of the sub-surfaces represented by forest canopy, forest soil, or forest snow. The total flux plus heat transfer determine the time evolution of the surface temperatures

$$
\begin{cases}
\dfrac{\partial T_{forc}}{\partial t} = & \dfrac{1}{C_{forc}}\Phi_{forc} \\
\dfrac{\partial T_{fors}}{\partial t} = & \dfrac{1}{(\rho C)_{fors}z_s}[\Phi_{fors} + \Lambda_s(T_{fors2} - T_{fors})] \\
\dfrac{\partial T_{forsn}}{\partial t} = & \dfrac{1}{(\rho C)_{forsn}z_{forsn}}[\Phi_{forsn} + \Lambda_{forsn}(T_{forsns} - T_{forsn})]
\end{cases}
\tag{24}
$$

where $(\rho C)_{fors}$ and $(\rho C)_{forsn}$ are volumetric heat capacities and Λ_s and Λ_{forsn} are heat transfer coefficients as defined in Sections 3.8 and 3.7, respectively. The heat capacity of the forest canopy is defined

as $C_{forc} = C_{veg}W_{veg} + C_w\rho_w w_{forc}$, where C_{veg} is the vegetative heat capacity, W_{veg} is the standing mass of the composite canopy, C_w is the specific heat of water, and w_{forc} is the amount of intercepted water (Verseghy et al., 1993). For the moment we assume the same vegetative heat capacity for all types of trees.

3.6 Open land and bare soil processes

The open land tile, which includes low vegetation and bare soil, has its separate energy balance represented by the surface temperature T_{opls}. The net radiation of the open land tile becomes $Rn_{opls} = (1 - \alpha_{opls})S\downarrow + \varepsilon_{opls}(L\downarrow + \sigma T_{opls}^4)$ and the energy flux becomes

$$H_{opls} = \rho c_p \frac{T_{opls} - T_{am}}{r_{aopl}}. \tag{25}$$

The evapotranspiration from low vegetation is parameterized as

$$E_{oplv} = \rho L_e h_{vopl} \frac{q_s(T_{opls}) - q_{am}}{r_{aopl} + r_{svopl}}, \tag{26}$$

where h_{vopl} is defined by replacing r_a with r_{aopl}, r_{sv} with r_{svopl}, and δ with δ_{oplv} in Equation 21, respectively.

The evaporation from bare soil is parameterized as

$$E_{opls} = \rho L_e \frac{q_s(T_{opls}) - q_{am}}{r_{aopl} + r_{ssopl}}. \tag{27}$$

3.7 Snow processes

A snow surface is very different from most other surfaces found over land. It is characterized by very high albedo and the snow itself has low heat capacity and very limited heat transfer capability. It is important to realistically simulate the fractional coverage of snow since snow is related to at least two important positive feedback loops. An overestimated fractional snow cover will lead to an overestimated area averaged albedo. This will reduce the amount of absorbed short wave radiation at the surface and cause a reduction in temperature which will be favourable for further snow accumulation. An underestimation of fractional snow cover during the spring will lead to an underestimated area averaged albedo which will tend to raise the temperature and accelerate the snow melt and a reduction in snow cover. Unfortunately snow cover is one of the most difficult snow related processes to simulate.

There are two separate snow packs in the present LSS: one on open land, where the fluxes directly communicate with the lowest model layer, and one in the forest, where the fluxes depend on the canopy air temperature and humidity. Except for the albedo, which is prognostic for open-land snow but constant for forest snow, the snow scheme is identical for the two snow packs.

3.7.1 Estimation of fractional snow cover

An open-land surface, initially with no snow cover, may be totally snow covered for only a small amount of snowfall. This would imply a very thin snow layer. Since snow has a low heat capacity such a thin layer could cause very rapid temperature changes in a numerical scheme and consequently numerical instability. Thus, for numerical reasons the fractional snow cover must increase gradually with increasing snow amount.

During the growing phase, the snow cover fraction, A_{sn}, is parameterized to asymptotically approach a maximum allowed snow cover fraction, A_{snlim} set to 0.95, as a function of the snow water equivalent sn according to

$$A_{sn} = A_{snlim} \tanh(100sn), \tag{28}$$

where the factor 100 is a constant controlling the rate of growth. A_{snlim} is set to less than one for numerical reasons but also because a landscape mostly includes rough surfaces and obstacles that always tend to create snow free areas. For a snow layer not reaching A_{snlim} in coverage the same formulation of snow cover is used during the melting phase.

If the snow pack has accumulated over a long enough time and reached over a certain limit in coverage, set to $A_{snlim} - 0.001$, the snow cover fraction during the melting phase is described differently. According to observations the snow cover for deep snow packs is better correlated with the ratio sn/sn_{max} than with sn itself, where sn_{max} is the maximum snow water equivalent reached during the snow season (Lindström and Gardelin, 1999). To simulate this process we store the memory of the snow pack in sn_{max}. When $A_{sn} = A_{snlim} - 0.001$ is reached sn_{max} is put equal to sn and during the rest of the snow season sn_{max} is kept larger than or equal to sn. During this period the snow cover fraction is parameterised according to

$$A_{sn} = \frac{sn}{sn_{max}\Delta_{snfrd}}, A_{sn} \leq A_{snlim}, \tag{29}$$

where Δ_{snfrd} is a snow fraction distribution factor. Thus, during snow melt A_{sn} will be kept at A_{snlim} until $sn = sn_{max}\Delta_{snfrd}$ is reached. According to observations of snow cover reported in Lindström and Gardelin (1999) Δ_{snfrd} is a function of orography. In mountainous areas Δ_{snfrd} tend to be higher than in less mountainous areas. Based on these observations the following formulation is used

$$\Delta_{snfrd} = 0.6 + 0.001\sigma_{orog}, \Delta_{snfrd} \leq 0.8, \tag{30}$$

where σ_{orog} is the degree of subgrid orography calculated as the standard deviation of the orography for a specific grid resolution based on the GTOPO30 database.

When the end of the snow season approaches, defined as when $sn^{\tau+1} < k_1 sn^{\tau}_{max}$, sn_{max} is gradually decreased to zero to allow for a new season to start following the function

$$sn^{\tau+1}_{max} = sn^{\tau}_{max} - (k_1 sn_{max} - sn^{\tau+1})(1-k)/k_1, \tag{31}$$

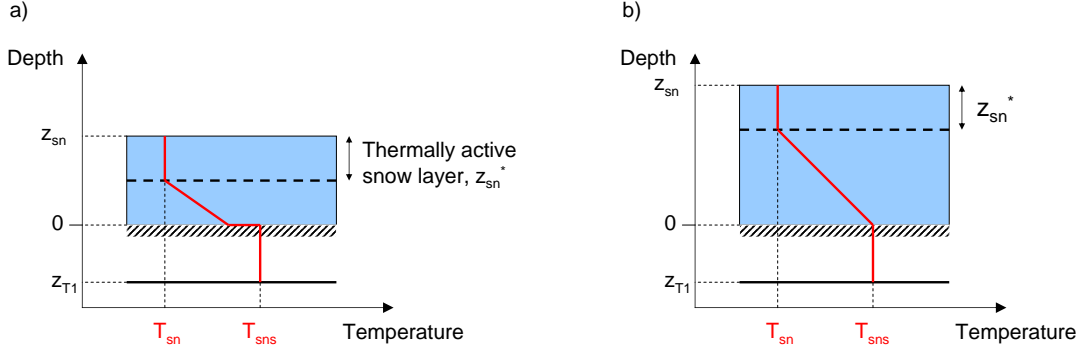where $k_1 = 0.2$ and $k = \exp(10^{-6}\Delta t)$.

Figure 2: Principal sketch of the assumed temperature profile in a thin (a) and in a thick (b) snow layer respectively.

3.7.2 Snow temperature

The purpose of the parameterization of snow in the present LSS is to give a reasonable surface temperature of the snow and a reasonable evolution of the snow pack including runoff of melt water. A correct surface temperature is especially important for the net long wave radiation on the diurnal time scale. On this time scale we assume that only the uppermost part of a thick snow layer is thermally active due to the limited heat transfer capability of snow. Thus, we use a bulk snow layer concept, only regarding the thermal properties of the snow in this layer. There will be a heat transfer also at the snow-soil interface which must be parameterized. Phase changes in the snow between snow and water are important to consider since such processes may have a strong influence on the temperature evolution. To account for these processes any snow melt water is partly kept in the snow as liquid water which can freeze again when the energy balance at the snow surface becomes negative.

Figure 2 shows the concept used describing the assumed temperature profile in the snow for a thin and for a deep snow layer, respectively. The depth of the thermally active layer is defined as $z_{sn}^* = \min(z_{sn}, z_{snmax})$, where z_{sn} is the actual snow depth and $z_{snmax} = 0.15$m is the maximum depth of the thermally active layer. The actual snow depth is defined as $z_{sn} = sn\rho_w/\rho_{sn}$, where ρ_{sn} and ρ_w are the densities of snow and water, respectively. ρ_{sn} is a prognostic variable in the present LSS as described in Appendix B.

The equation for the snow temperature is as follows:

$$\frac{\partial T_{sn}}{\partial t} = \frac{1}{(\rho C)_{sn} z_{sn}} \left[\Phi_{sn} + \Lambda_{sn}(T_{sns} - T_{sn}) \right],\qquad(32)$$

where $(\rho C)_{sn} = (\rho C)_{ice}\rho_{sn}/\rho_{ice}$ is the volumetric heat capacity of the snow and $(\rho C)_{ice}$ is the volumetric heat capacity for ice. $\Phi_{sn} = Rn_{sn} + H_{sn} + E_{sn}$ is the sum of the energy fluxes at the snow surface, net radiation and sensible and latent heat fluxes, respectively, defined as

$$Rn_{sn} = (1 - \alpha_{sn})S\downarrow + \varepsilon_{sn}(L\downarrow - \sigma T_{sn}^4),\qquad(33)$$

$$H_{sn} = \rho c_p \frac{T_{sn} - T_{am}}{r_{asn}},\qquad(34)$$

13

$$E_{sn} = \rho L_e \frac{q_s(T_{sn}) - q_{am}}{r_{asn}}. \tag{35}$$

Note that these equations refer to the open land snow and must be replaced by the corresponding forest equations in the case of forest snow. The snow albedo, α_{sn}, is defined in Appendix B.

The snow temperature in the layer below the thermally active layer is in principal unknown which means that the heat transfer at the snow-soil interface is parameterised using a heat transfer coefficient Λ_{sn} between the snow and the underlying soil layer. Basically it is assumed that the heat transfer at the snow-soil interface decreases with the depth of the snow layer. Λ_{sn} is simply a weighted average of the heat transfer coefficients of snow and soil, respectively, defined as

$$\Lambda_{sn}^{-1} = 0.5 \frac{z_{sn}}{\lambda_{sn}} + 0.5 \frac{z_{T1}}{\lambda_T}, \tag{36}$$

where $\lambda_{sn} = \lambda_{ice}(\rho_{sn}/\rho_{ice})^{1.88}$ and λ_T is defined in Equation 42 and $\lambda_{ice} = 2.2$ W m^{-1} K^{-1}.

The snow temperature equation is part of a heat conduction problem including the soil temperature equations. The resulting equation system is solved implicitly. In the case of phase changes, i.e. melting of snow or freezing of liquid water in the snow, the time step is divided into two parts, one where the temperature of the snow is kept constant and one where the snow temperature is allowed to change.

3.7.3 Phase changes in snow

Two types of phase changes can take place in the snow pack; at positive energy balance the snow temperature increases until the melting temperature is reached and melting starts, while at negative energy balance any liquid water in the snow can partly refreeze at the same time as the snow temperature drops. One can use different strategies to numerically solve this phase-change problem. We have chosen to divide the time step into two parts which means that upon melting, one part of the time step is used for increasing the temperature and the other part is used to melt snow while keeping the snow temperature at the melting point. Upon freezing, one part of the time step is used to freeze liquid water while keeping the snow temperature constant and the other part is used to decrease the snow temperature.

The total energy per unit time available for the snow is

$$\Phi_{tot} = \Phi_{sn} + \Lambda_{sn}(T_{sns} - T_{sn}). \tag{37}$$

If $\Phi_{tot} > 0$, we estimate the time, Δt_{dtemp}, it takes to bring T_{sn} to T_{melt} using Equation 32. If $\Delta t_{dtemp} \geq \Delta t$ the melting temperature is not reached and the snow temperature is calculated using Equation 32 with $\Delta t_{dtemp} = \Delta t$. If $\Delta t_{dtemp} < \Delta t$ Equation 32 is used to bring T_{sn} to T_{melt} and then Φ_{tot} is used during the rest of the time step, $\Delta t_{dphase} = \Delta t - \Delta t_{dtemp}$, to melt snow while T_{sn} is kept at the melting temperature. The amount of melted snow, or water, becomes

$$sn_{mel} = \frac{\Delta t_{dphase}\Phi_{tot}}{\rho_w L}, \tag{38}$$

14

where L is the latent heat of freezing. This amount is used to increase the amount of liquid water kept in the snow, w_{sn}, until it reaches a maximum allowed amount, $w_{snsat} = \Delta_{snsat}sn$, where Δ_{snsat} is set to 10%. Any excess liquid water goes to the soil.

At negative energy balance for the snow, i.e. $\Phi_{tot} < 0$, the snow temperature should drop but if the liquid water content is non-zero we should also freeze some of the water. In contrast to the straight forward melting processes the parameterisation of the freezing process is not as obvious in the case of $w_{sn} > 0$. How much of the liquid water that should be frozen during a certain time does, in principle, depend on where the water is located in the snow layer and how the characteristics of the heat transfer in the snow looks like. With a snow model as simple as the one described here it is impossible to make any physically valid estimation on this amount. Thus, we are let out to some estimation based on assumptions. The assumptions made here are based on the fact that snow melt mainly occurs at the top of the snow layer and that the melt water is located where melting occurs. The larger the amount of melt water in the snow the deeper it penetrates. We estimate a fraction, Δ_{freeze}, of the liquid water amount that is allowed to freeze according to

$$\Delta_{freeze} = \min\left(\frac{sn_{freeze}\rho_{sn}}{\rho_w} \frac{\Delta_{snsat}}{w_{sn}}, 1 \right),\tag{39}$$

where sn_{freeze} is an assumed depth of snow over which freezing is allowed to be active, set to 0.03 m. In other words, the equivalent water amount corresponding to sn_{freeze} is $sn_{freeze}\rho_{sn}/\rho_w$. The corresponding maximum liquid water amount allowed is given by $sn_{freeze}\rho_{sn}/\rho_w\Delta_{snsat}$ which is related to the actual liquid water amount, w_{sn}. The value of sn_{freeze} must be estimated by trial and error examining the simulated snow temperature against observations. Δ_{freeze} is used to calculate the fraction of the time step to be used for freezing of water, $\Delta t_{dphase} = \Delta_{freeze}\Delta t$. During this time the snow temperature is kept constant. Cooling of the snow temperature takes place during the rest of the time step, $\Delta t_{dtemp} = \Delta t - \Delta t_{dphase}$, by applying Equation 32. If the available water is less than the corresponding water given by Δt_{dphase}, the time for freezing of water is reduced.

The change in open-land snow water equivalent is as follows:

$$sn^{\tau+1} = sn^{\tau} + \frac{\Delta t}{\rho_w}\left[A_{sn}(F + P_{sn-}) + A_{opl}(F + P_{opl-} - F_{opl+}) + A_{sn}\frac{E_{sn}}{L_e} \right] - sn_{mel},\tag{40}$$

which includes the three phase changes P_{sn-}, rain freezing on cold snow, P_{opl-}, rain freezing on cold ground and F_{opl+}, snow melting on warm ground. F denotes snowfall (kg m^{-2}s^{-1}). The change in forest snow water equivalent is given by a corresponding equation.

3.8 Soil processes

The soil is characterized by its texture and water content. The present scheme uses seven different texture classes based on the geographical distribution of soil types FAO-Unesco (1981) digitized for Europe by the German Weather Service. These classes are sand, loam, clay, sandy loam, silt loam, sandy clay, and peat. The hydraulic properties for each soil type are based on Clapp and Hornberger (1978) and McCumber and Pielke (1981) and are specified in terms of total porosity θ_{sat} (m^{3}m^{-3}), field capacity θ_{fc} (m^{3}m^{-3}), wilting point θ_{wi} (m^{3}m^{-3}), matric potential at saturation ψ_{sat} (m), hydraulic conductivity at saturation γ_{sat} (m s^{-1}), Clapp and Hornberger soil parameter b, and volumetric dry soil heat capacity $(\rho C)_s$ (Jm^{-3}K^{-1}).

3.8.1 Soil temperature

The soil heat transfer equation applied for each soil layer can be written as

$$[(\rho C)_{s\theta} + \Delta C_{fs}]\frac{\partial T_s}{\partial t} = \frac{\partial}{\partial z}\left(\phi^{t,b} + \lambda_T \frac{\partial T_s}{\partial z}\right). \tag{41}$$

Here $(\rho C)_{s\theta}$ is the volumetric wet soil heat capacity for a soil moisture content of θ ($m^3 m^{-3}$) defined as $(\rho C)_{sw} = (\rho C)_s + \theta \rho_w C_w$.

The present LSS does not include the solid phase of soil water which means that e.g. the thermal process related to the latent heat of fusion/freezing is absent. This process is important since it acts to delay the soil cooling in autumn and the soil warming in spring. To simulate this effect we apply a modification of the soil heat capacity, ΔC_{fs}, as suggested by Viterbo et al. (1999), which increases the total soil heat capacity in the temperature range -3 to +1°C.

The heat conductivity λ_T depends on the soil water content as described by McCumber and Pielke (1981)

$$\lambda_T(\theta) = -a\psi_{sat}^{-1/\log 10}\left(\frac{\theta_{sat}}{\theta}\right)^{-b/\log 10}. \tag{42}$$

Here a is an empirical soil thermal conductivity parameter.

The top boundary condition, ϕ^t, is represented by the total flux at the surface, ϕ_{fors} or ϕ_{opls} in the cases of forest soil or open-land soil, respectively, or the heat transfer at the soil/snow interface in the cases of snow covered soil in the forest or at the open land as defined in Section 3.7. At the bottom a zero-flux condition is assumed, i.e. $\phi^b = 0$.

Since there are four different top boundary conditions for the soil we will have four soil columns with different evolutions of their soil temperature profiles. The soil is divided into five layers in the vertical with respect to temperature which thus results in 20 prognostic soil temperatures. If the fractional snow cover changes during a time step the soil temperatures have to be adjusted accordingly to avoid an artificial change of the total heat content of the soil.

3.8.2 Soil moisture, drainage and runoff

The vertical transport of water in the unsaturated soil is usually expressed using Richards equation (Hillel, 1980)

$$\frac{\partial \theta}{\partial t} = \frac{\partial}{\partial z}\left(\lambda\frac{\partial \theta}{\partial z}\right) - \frac{\partial \gamma}{\partial z} + S(\theta, z), \tag{43}$$

where λ is the hydraulic diffusivity ($m^2 s^{-1}$), γ is the hydraulic conductivity (ms^{-1}), and $S(\theta, z)$ is a volumetric source/sink term ($m^3 m^{-3} s^{-1}$). The hydraulic diffusivity is parameterized according to McCumber and Pielke (1981)

$$\lambda = \frac{b\gamma_{sat}(-\psi_{sat})}{\theta_{sat}}\left(\frac{\theta}{\theta_{sat}}\right)^{b+2}. \tag{44}$$

The volumetric source/sink term generally includes effects of precipitation, runoff, root extraction, and phase changes of ice to liquid water. However, as described above we do not explicitly include any phase changes of ice to liquid water in the soil but instead we parameterize the effect that soil ice would have had on soil heat capacity and root extraction. In the present LSS we replace the hydraulic conductivity term, $\partial \gamma / \partial z$, in Equation 43 with a drainage/runoff parameterization as part of the $S(\theta, z)$ term. The final sources and sinks in $S(\theta, z)$ then become; supply of water at the soil surface, $S^w(z_0)$, evaporation/condensation at the soil surface, $S^e(\theta, z_0)$, loss due to root extraction, $S^{re}(\theta, z_d)$, and drainage/runoff, $S^{dr}(\theta, z_d)$, at each soil layer/interface z_d. No lateral transport of water exists in the scheme. The supply of water at the soil surface is represented by contributions from rainfall, snow-melt water, and throughfall from vegetation. The evaporation/condensation at the soil surface is represented by two terms; one for the forest floor soil, which is the E_{fors} equation in Equation array 22, and one for the open land soil, Equation 27.

The loss due to root extraction is given by the transpiration parts of Equations 22(E_{forc}) and 26, i.e. with the transpiration components of the Halstead coefficients, h^{tr}_{vfor} and h^{tr}_{vopl}.

The drainage/runoff parameterization is based on the so called β-formulation as used in the hydrological HBV model (Lindström et al., 1997). The drainage can then be written as a source/sink term

$$S^{dr}(\theta, z_n) = S^{dr}(\theta, z_{n-1}) \left(\frac{\theta - \theta_{wi}}{\theta_{fc} - \theta_{wi}} \right)^{\beta}, \tag{45}$$

where the upper boundary condition $S^{dr}(\theta, z_0) = S^w(z_0)$ and the resulting runoff is given by $S^{dr}(\theta, z_2)$. The exponent β set to zero would imply a grid square with no water holding capacity at all while a high β value indicates such homogeneous conditions that the whole grid square may be regarded as a bucket that overflows when its field capacity is reached. β is thus more an index of heterogeneity than of soil property. β is a tuning parameter and in the present model we use the same value as is used in the HBV model, which is 2 for both soil layers (Bergström and Graham, 1998).

A Aerodynamic resistances within the forest

The parameterisation of the bulk aerodynamic resistance $r_b = 1/g_b$ is based on Choudhury and Monteith (1988), where the conductance between the canopy and the canopy air, g_b, is defined as

$$g_b = \frac{2LAIa}{\alpha'} \left(\frac{u_{for}}{lw}\right)^{1/2} [1 - \exp(-\alpha'/2)]. \tag{46}$$

The conductance is modified with a free convection correction according to Sellers et al. (1986)

$$g_b = g_b + \frac{LAI}{890} \left(\frac{T_{forc} - T_{fora}}{lw}\right)^{1/4}. \tag{47}$$

The aerodynamic resistance r_d is based on Choudhury and Monteith (1988)

$$r_d = \frac{z_{for} \exp(\alpha)}{\alpha K(z_{for})} [\exp(-\alpha z_0'/z_{for}) - \exp(-\alpha(d + z_0)/z_{for})], \tag{48}$$

where

$$K(z_{for}) = k(z_{for} - d)u_{*for} = \frac{k^2(z_{for} - d)u}{\ln \frac{z_{for}-d}{z_0}}. \tag{49}$$

The displacement height is defined as (Choudhury and Monteith, 1988):

$$d = 1.1z_{for} \ln[1 + (c_d LAI_f)^{1/4}] \tag{50}$$

where the leaf drag coefficient c_d is defined as (Sellers et al., 1996):

$$c_d = 1.328 \left[\frac{2}{\text{Re}^{1/2}}\right] + 0.45 \left[\frac{1}{\pi}(1 - \chi_L)\right]^{1.6} \tag{51}$$

where χ_L is the Ross-Goudriaan leaf angle distribution function, which has been estimated according to Monteith (1975) (see Table 1), and Re is the Reynolds number defined as

$$\text{Re} = \frac{u_l lw}{\upsilon}. \tag{52}$$

The unstable transfer correction for $r_d = r_d/\psi_H$ according to Sellers et al. (1986), where

$$\psi_H = \left[1 + 9\frac{T_{fors} - T_{fora}}{T_{fors}u_{for}^2} z_{for}\right]^{1/2}. \tag{53}$$

For the estimations of r_b and r_d the friction velocity at the forest tile, u_{*for}, is needed as well as the wind speed at the top of the forest, i.e. u_{for} at z_{for}. u_{*for} is estimated from the drag coefficient of momentum calculated as in Equation 3 but with z_{0h} replaced by z_{0m}. u_{for} is then reached in two steps: firstly the wind speed u_{trans} at a transition level z_{trans}, located between z_{am} and z_{for}, is calculated as

$$u(z_{trans}) = \frac{u_{*for}}{k} \left[\ln \frac{z_{trans} - d}{z_{0m}} - \Psi_m \left(\frac{z_{trans} - d}{L} \right) \right], \tag{54}$$

where z_{trans} is defined as

$$z_{trans} = z_{for} + 11.785 z_{0m}. \tag{55}$$

Secondly, $u_{for} = u(z_{trans}) - G_2 \Delta u(z_{trans}, z_{for})$, where $\Delta u(z_{trans}, z_{for}) = u(z_{trans}) - u(z_{for})$ and G_2 is an adjustment factor which is equal to 0.75 according to Xue et al. (1991).

Table 1: Surface independent parameters

Symbol	Definition	Unit	Value	Reference	Comment
g	Acceleration of gravity	m s^{-2}	9.81		
G_2	Adjustment factor	-	0.75	Xue et al. (1991)	Eq. 13
k	von Karman constant	-	0.4		
a		m s$^{-1/2}$	0.01	Choudhury and Monteith (1988)	Eq. 26
α'	attenuation coeff. for wind	-	3	Choudhury and Monteith (1988)	p 386
lw	leaf width	m	0.02		
α	attenuation coeff. for mom.	-	2	Choudhury and Monteith (1988)	p 386
z_0'	roughness of soil surface	m	0.007		
χ_L	Ross-Goudriaan leaf angle dist.	-	0.12	Monteith (1975)	p 26
u_l	Typical local wind speed	m s^{-1}	1	Sellers et al. (1996)	Eq. B7
υ	Kinematic viscos. of air	m^2 s^{-1}	0.15×10^{-4}		

B Snow density and snow albedo

B.1 Snow density

The density of the snow increases exponentially with time towards a maximum value as long as no fresh snow is added by snowfall. The total density of the snow pack is a weighted value of the dry snow and of the liquid water content. Assuming that we have the density of the dry snow calculated, ρ_{snd}, which compare to the water equivalent of the dry snow, sn_d, we can combine that with any snowfall, F, during the time step to a temporary new dry snow density

$$\rho_{snd}^* = \frac{sn_d^\tau \rho_{snd}^\tau + (\Delta t F / \rho_w) \rho_{snmin}}{sn_d^\tau + (\Delta t F / \rho_w)}, \tag{56}$$

where $\rho_{snmin} = 100$ kg m^{-3} is the minimum density of dry snow. The new value of the dry snow density becomes

$$\rho_{snd}^{\tau+1} = (\rho_{snd}^* - \rho_{snmax}) \exp(-\tau_f \Delta t / \tau_1) + \rho_{snmax}, \tag{57}$$

where $\rho_{snmax} = 300$ kg m^{-3} is the maximum density of dry snow. The time scales $\tau_1 = 86400$ s and $\tau_f = 0.24$ give an e-folding time of about 4 days. Combining the new dry snow density with the liquid water content in the snow gives the total density of the snow

$$\rho_{sn}^{\tau+1} = \Delta_{snd}^{\tau+1}\rho_{snd}^{\tau+1} + (1 - \Delta_{snd}^{\tau+1})\rho_w, \qquad (58)$$

where Δ_{snd} is the fraction of dry snow to total snow, i.e. $\Delta_{snd} = (sn - w_{sn})/sn$.

B.2 Snow albedo

The net radiation balance at the surface for open land snow is given by $Rn_{sn} = (1 - \alpha_{sn})S{\downarrow} + \varepsilon_{sn}(L{\downarrow} - \sigma T_{sn}^4)$, where the snow albedo, α_{sn}, for open-land snow is a prognostic variable. The albedo for snow in the forest is put constant to 0.2. The parameterisation of snow albedo evolution with time is based on Verseghy (1991) and Douville et al. (1995). For non-melting conditions the albedo decreases linearly with time according to

$$\alpha_{sn}^{\tau+1} = \alpha_{sn}^{\tau} - \tau_a\Delta t/\tau_1, \qquad (59)$$

where $\tau_a = 0.008$, while for melting conditions the albedo decreases exponentially with time according to

$$\alpha_{sn}^{\tau+1} = [\alpha_{sn}^{\tau} - \alpha_{min}]\exp(-\tau_f\Delta t/\tau_1) + \alpha_{min}, \qquad (60)$$

where $\alpha_{min} = 0.50$. If the snowfall exceeds $1/3600$ kg m^{-2} s^{-1} the snow albedo is set to $\alpha_{sn}^{\tau+1} = \alpha_{max} = 0.85$.

C Diagnostic quantities

Except for prognostic variables at the surface and at atmospheric model levels there is a need to calculate diagnostic variables that correspond to common observed quantities. Some of the most important diagnostic variables are air temperature and specific humidity at 2m height ($T2m$ and $q2m$) and wind speed components at 10m height ($u10$ and $v10$). The calculation of these diagnostic variables for a given height z are based on Monin-Obukhov similarity theory:

$$\begin{cases} u(z) = \frac{u_*}{k}\left[\ln\frac{z}{z_{0m}} - \Psi_m\left(\frac{z}{L}\right)\right] \\ v(z) = \frac{v_*}{k}\left[\ln\frac{z}{z_{0m}} - \Psi_m\left(\frac{z}{L}\right)\right] \\ T(z) = T_s + \frac{\theta_*}{k}\left[\ln\frac{z}{z_{0h}} - \Psi_h\left(\frac{z}{L}\right)\right] \\ q(z) = q_s + \frac{q_*}{k}\left[\ln\frac{z}{z_{0q}} - \Psi_q\left(\frac{z}{L}\right)\right] \end{cases} \qquad (61)$$

where u_* and v_* are friction velocities, θ_* and q_* are temperature and humidity scales, respectively, k is the von Karman's constant, z_{0m}, z_{0h} and z_{0q} are roughness lengths for momentum, heat and humidity, respectively, L is the Monin-Obukhov length, T_s and q_s are surface values, and Ψ_x represents analytic stability functions for momentum, heat and humidity, respectively.

In RCA3 these equations are approximated to (Woetmann Nielsen, 1987):

Stable case:

Stable case:

$$\begin{cases} u(z) = \frac{u_*}{k}\ln\frac{z}{z_{0m}} + u_{am}\left[1 - \exp\left(-\frac{1}{kRi_{cr}}\frac{u_*}{u_{am}}\frac{z}{L}\right)\right] \\ v(z) = \frac{v_*}{k}\ln\frac{z}{z_{0m}} + v_{am}\left[1 - \exp\left(-\frac{1}{kRi_{cr}}\frac{v_*}{v_{am}}\frac{z}{L}\right)\right] \\ T(z) = T_s + \frac{\theta_*}{k}\ln\frac{z}{z_{0h}} + (T_{am} - T_s)\left[1 - \exp\left(-\frac{1}{kRi_{cr}}\frac{\theta_*}{T_{am}}\frac{z}{L}\right)\right] \\ q(z) = q_s + \frac{q_*}{k}\ln\frac{z}{z_{0q}} + (q_{am} - q_s)\left[1 - \exp\left(-\frac{1}{kRi_{cr}}\frac{q_*}{q_{am}}\frac{z}{L}\right)\right] \end{cases} \tag{62}$$

where $Ri_{cr} = 0.25$, $z_{0q} = z_{0h}$ and subindex am represents lowest atmospheric model level.

Unstable case:

$$\begin{cases} u(z) = \frac{u_*}{k}\left[\ln\frac{z}{z_{0m}} - \left(\ln\frac{1+x^2}{2} + 2\ln\frac{1+x}{2} - 2\tan^{-1}x + \frac{\pi}{2}\right)\right] \\ v(z) = \frac{v_*}{k}\left[\ln\frac{z}{z_{0m}} - \left(\ln\frac{1+x^2}{2} + 2\ln\frac{1+x}{2} - 2\tan^{-1}x + \frac{\pi}{2}\right)\right] \\ T(z) = T_s + \frac{\theta_*}{k}\left[\ln\frac{z}{z_{0h}} - 2\ln\frac{1+y}{2}\right] \\ q(z) = q_s + \frac{q_*}{k}\left[\ln\frac{z}{z_{0q}} - 2\ln\frac{1+y}{2}\right] \end{cases} \tag{63}$$

where $x = (1 - 15z/L)^{1/4}$ and $y = (1 - 9z/L)^{1/2}$.

The Monin-Obukhov length is defined as

$$L = -\frac{u_*^3 T}{kg\overline{w'\theta_v'}} = \frac{u_*^3}{kgH_v/c_p}\frac{p_s - dph}{R_d} = \frac{u_*^3}{kgH_v/(\rho c_p)}T_{am} \tag{64}$$

where the buoyancy flux H_v is defined as

$$H_v = H + 0.61c_p T_{am}E/L_e. \tag{65}$$

$u10$, $v10$, $T2m$ and $q2m$ are all calculated separately for each tile. Any diagnostic values representing groups of tiles or the whole grid square are calculated as area averaged values.

D   Numerical details

D.1   Solving for T_{fora} and q_{fora}

The heat fluxes in Equations 22 are functions of T_{fora} or q_{fora} but so are also the aerodynamic resistances included in the equations. Thus, the equilibrium value of T_{fora} with respect to the temperatures T_{forc}, T_{fors}, T_{forsn}, and T_{am} has to be solved for iteratively. T_{fora} is solved from the relationship

$$H_{for} = H_{forc} + (1 - A_{forsn})H_{fors} + A_{forsn}H_{forsn} \tag{66}$$

which gives

$$T_{fora} = \frac{\frac{T_{am}}{r_{afor}} + \frac{(1 - A_{forsn})T_{fors} + A_{forsn}T_{forsn}}{r_d} + \frac{T_{forc}}{r_b}}{\frac{1}{r_{afor}} + \frac{1}{r_d} + \frac{1}{r_b}}. \tag{67}$$

q_{fora} is solved for in a similar manner with a corresponding equation for latent heat fluxes as the one for sensible heat fluxes in Equation 66.

D.2   Solving the heat conduction

Once the fluxes are computed we solve the heat conduction for each tile, using the implicit method of Richtmeyer and Morton (1967). The degree of implicity is set to 0.5, except for the fast variables, T_{forc}, T_{fors}, T_{forsn} and T_{opls}, which are treated fully implicitly.

References

Beljaars, A. C. M., Viterbo, P., 1994. The sensitivity of winter evaporation to the formulation of aerodynamic resistance in the ECMWF model. Boundary-Layer Meteorol. 71, 135–149.

Bergström, S., Graham, L. P., 1998. On the scale problem in hydrological modelling. J. Hydrology 211, 253–265.

Bringfelt, B., Räisänen, J., Gollvik, S., Lindström, G., Graham, L. P., Ullerstig, A., 2001. The land surface treatment for the Rossby Centre regional atmosphere climate model - version 2. Reports of Meteorology and Climatology 98, SMHI, SE-601 76 Norrköping, Sweden.

Chen, F., Janjić, Z., Mitchell, K., 1997. Impact of atmospheric surface-layer parameterizations in the new land-surface scheme of the NCEP Eta model. Boundary-Layer Meteorol. 85, 391–421.

Choudhury, B. J., Monteith, J. L., 1988. A four-layer model for the heat budget of homogeneous land surfaces. Q. J. R. Meteorol. Soc. 114, 373–398.

Clapp, R. B., Hornberger, G. M., 1978. Empirical equations for some soil hydraulic properties. Water Resources Res. 14, 601–604.

Deardorff, J. W., 1978. Efficient prediction of ground surface temperature and moisture, with inclusion of a layer of vegetation. J. Geophys. Res. 83, 1889–1903.

Dickinson, R. E., 1984. Modeling evapotranspiration for three dimensional global climate models. Climate Processes and Climate Sensitivity. Geophys. Monogr. 29, 58–72.

Douville, H., Royer, J. F., Mahfouf, J. F., 1995. A new snow parameterization for the meteo-france climate model. Part I: validation in stand-alone experiments. Climate Dyn. 12, 21–35.

FAO-Unesco (Ed.), 1981. Soil map of the world: Vol. 5, Europe. Unesco-Paris.

Hagemann, S., Botzet, M., Dümenil, L., Machenhauer, B., 1999. Derivation og global GCM boundary conditions from 1 km land use satellite data. Tech. Rep. 289, Max-Planck-Institute for Meteorology, Hamburg, Germany.

Hillel, D., 1980. Fundamentals of Soil Physics. Academic Press, New York.

Jarvis, P. G., 1976. The interpretation of the variations in leaf water potential and stomatal conductance found in canopies in the field. Phil. Trans. Roy. Soc. London B273, 593–610.

Kjellström, E., Bärring, L., Gollvik, S., Hansson, U., Jones, C., Samuelsson, P., Rummukainen, M., Ullerstig, A., Willén, U., Wyser, K., 2006. A 140-year simulation of European climate with the new version of the Rossby Centre regional atmospheric climate model (RCA3). Reports Meteorology and Climatology 108, SMHI, SE-601 76 Norrköping, Sweden.

Koster, R. D., Suarez, M. J., 1992. A comparative analysis of two land-surface heterogeneity representations. J. Climate. 5, 1379–1390.

Lindström, G., Gardelin, M., 1999. A simple snow parameterization scheme intended for the RCA model based on the HBV runoff model. SWECLIM Newsletter 6, SMHI, Sweden, 16–20.

Lindström, G., Johansson, B., Persson, M., Gardelin, M., Bergström, S., 1997. Development and test of the distributed HBV-96 hydrological model. J. Hydrology 201, 272–288.

Louis, J. F., Tiedtke, M., Geleyn, J. F., 1981. A short history of the PBL parameterization at ECMWF. In: Workshop on Boundary Layer Parameterization. European Centre for Medium-Range Weather Forecasts, Reading, U.K.

McCumber, M. C., Pielke, R. A., 1981. Simulation of the effects of surface fluxes of heat and moisture in a mesoscale numerical model 1. Soil layer. J. Geophys. Res. 86, 9,929–9,938.

Mölder, M., Lindroth, A., 1999. Thermal roughness length of a boreal forest. Agric. Forest Meteorol. 98–99, 659–670.

Monteith, J. L. (Ed.), 1975. Vegetation and the atmosphere. Vol. 1. Academic Press.

Noilhan, J., Planton, S., 1989. A simple parameterization of land surface processes for meteorological models. Mon. Wea. Rev. 117, 536–549.

Richtmeyer, R. D., Morton, K. W., 1967. Difference Methods for Initial-Value Problems. Interscience Publishers.

Samuelsson, P., Bringfelt, B., Graham, L. P., 2003. The role of aerodynamic roughness for runoff and snow evaporation in land-surface schemes — comparison of uncoupled to coupled simulations. Global Planetary Change 38, 93–99.

Sellers, P. J., Mintz, Y., Sud, Y. C., Dalcher, A., 1986. A simple biosphere model (SiB) for use within general ciculation models. J. Atmos. Sci. 43, 505–531.

Sellers, P. J., Randall, D. A., Collatz, G. J., Berry, J. A., Field, C. B., Dazlich, D. A., Zhang, C., Collelo, G. D., Bounoua, L., 1996. A revised land surface parameterization (SiB2) for atmospheric GCMs. Part I: Model formulation. J. Climate 9, 676–705.

van den Hurk, B., Viterbo, P., 2003. The Torne-Kalix PILPS2E experiment as a test bed for modifications to the ECMWF land surface scheme. Global Planetary Change 38, 165–173.

van den Hurk, B. J. J. M., Viterbo, P., Beljaars, A. C. M., Betts, A. K., 2000. Offline validation of the ERA40 surface scheme. Technical Memorandum 295, ECMWF.

Verseghy, D. L., 1991. CLASS – A Canadian land surface scheme for GCMs, I. Soil model. Int. J. Climatol. 11, 111–133.

Verseghy, D. L., McFarlane, N. A., Lazare, M., 1993. CLASS – A Canadian land surface scheme for GCMs, II. Vegetation model and coupled runs. Int. J. Climatol. 13, 347–370.

Viterbo, P., Beljaars, A., Teixeira, J., 1999. The representation of soil moisture freezing and its impact on the stable boundary layer. Quart. J. Roy. Meteorol. Soc. 125, 2401–2426.

Viterbo, P., Beljaars, C. M., 1995. An improved land surface parameterization scheme in the ECMWF model and its validation. J. Climate 8, 2716–2748.

Woetmann Nielsen, N., 1987. An approximate method for calculation of surface fluxes in an unstable atmospheric surface layer. HIRLAM Technical Note 1.

Xue, Y., Sellers, P. J., Kinter, J. L., Shukla, J., 1991. A simplified Biosphere Model for Global Climate Studies. J. Climate 4, 345–364.

Zilitinkevich, S., 1995. Non-local turbulent transport: Pollution dispersion aspects of coherent structure of convective flows. In: Power, H., Moussiopoulos, N., Brebbia, C. A. (Eds.), Air pollution III - Volume I. Air pollution theory and simulation. Computational Mechanics Publications, Southampton, Boston, pp. 53–60.

SMHIs publiceringar

SMHI ger ut sex rapportserier. Tre av dessa, R-serierna är avsedda för internationell publik och skrivs därför oftast på engelska. I de övriga serierna används det svenska språket.

Seriernas namn	Publiceras sedan
RMK (Rapport Meteorologi och Klimatologi)	1974
RH (Rapport Hydrologi)	1990
RO (Rapport Oceanografi)	1986
METEOROLOGI	1985
HYDROLOGI	1985
OCEANOGRAFI	1985

I serien METEOROLOGI har tidigare utgivits:

1985

1 Hagmarker, A. (1985)
Satellitmeteorologi.

2 Fredriksson, U., Persson, Ch., Laurin, S. (1985)
Helsingborgsluft.

3 Persson, Ch., Wern, L. (1985)
Spridnings- och depositionsberäkningar för av fallsförbränningsanläggningar i Sofielund och Högdalen.

4 Kindell, S. (1985)
Spridningsberäkningar för SUPRAs anläggningar i Köping.

5 Andersson, C., Kvick, T. (1985)
Vindmätningar på tre platser på Gotland. Utvärdering nr 1.

6 Kindell, S. (1985)
Spridningsberäkningar för Ericsson, Ingelstafabriken.

7 Fredriksson, U. (1985)
Spridningsberäkningar för olika plymlyft vid avfallsvärmeverket Sävenäs.

8 Fredriksson, U., Persson, Ch. (1985)
NO_x- och NO_2-beräkningar vid Vasaterminalen i Stockholm.

9 Wern, L. (1985)
Spridningsberäkningar för ASEA transformers i Ludvika.

10 Axelsson, G., Eklind, R. (1985)
Ovädret på Östersjön 23 juli 1985.

11 Laurin, S., Bringfelt, B. (1985)
Spridningsmodell för kväveoxider i gatumiljö.

12 Persson, Ch., Wern, L. (1985)
Spridnings- och depositionsberäkningar för avfallsförbränningsanläggning i Sofielund.

13 Persson, Ch., Wern, L. (1985)
Spridnings- och depositionsberäkningar för avfallsförbränningsanläggning i Högdalen.

14 Vedin, H., Andersson, C. (1985)
Extrema köldperioder i Stockholm.

15 Krieg, R., Omstedt, G. (1985)
Spridningsberäkningar för Volvos planerade bilfabrik i Uddevalla.

16 Kindell, S. Wern, L. (1985)
Luftvårdsstudie avseende industrikombinatet i Nynäshamn (koncentrations- och luktberäkningar).

17 Laurin, S., Persson, Ch. (1985)
Beräknad formaldehydspridning och deposition från SWEDSPANs spånskivefabrik.

18 Persson, Ch., Wern, L. (1985)
Luftvårdsstudie avseende industrikombinatet i Nynäshamn – depositionsberäkningar av koldamm.

19   Fredriksson, U. (1985)
Luktberäkningar för Bofors Plast i
Ljungby, II.

20   Wern, L., Omstedt, G. (1985)
Spridningsberäkningar för Volvos
planerade bilfabrik i Uddevalla - energi-
centralen.

21   Krieg, R., Omstedt, G. (1985)
Spridningsberäkningar för Volvos
planerade bilfabrik i Uddevalla -
kompletterande beräkningar för fabrikerna.

22   Karlsson, K.-G. (1985)
Information från Meteosat - forskningsrön
och operationell tillämpning.

23   Fredriksson, U. (1985)
Spridningsberäkningar för AB Åkerlund &
Rausings fabrik i Lund.

24   Färnlöf, S. (1985)
Radarmeteorologi.

25   Ahlström, B., Salomonsson, G. (1985)
Resultat av 5-dygnsprognos till ledning för
isbrytarverksamhet vintern 1984-85.

26   Wern, L. (1985)
Avesta stadsmodell.

27   Hultberg, H. (1985)
Statistisk prognos av yttemperatur.

1986

1   Krieg, R., Johansson, L., Andersson, C.
(1986)
Vindmätningar i höga master, kvartals-
rapport 3/1985.

2   Olsson, L.-E., Kindell, S. (1986)
Air pollution impact assessment for the
SABAH timber, pulp and paper complex.

3   Ivarsson, K.-I. (1986)
Resultat av byggväderprognoser -
säsongen 1984/85.

4   Persson, Ch., Robertson, L. (1986)
Spridnings- och depositionsberäkningar
för en sopförbränningsanläggning i
Skövde.

5   Laurin, S. (1986)
Bilavgaser vid intagsplan - Eskilstuna.

6   Robertson, L. (1986)
Koncentrations- och depositions-
beräkningar för en sopförbrännings-
anläggning vid Ryaverken i Borås.

7   Laurin, S. (1986)
Luften i Avesta - föroreningsbidrag från
trafiken.

8   Robertson, L., Ring, S. (1986)
Spridningsberäkningar för bromcyan.

9   Wern, L. (1986)
Extrema byvindar i Orrefors.

10   Robertson, L. (1986)
Koncentrations- och depositions-
beräkningar för Halmstads avfalls-
förbränningsanläggning vid Kristinehed.

11   Törnevik, H., Ugnell (1986)
Belastningsprognoser.

12   Joelsson, R. (1986)
Något om användningen av numeriska
prognoser på SMHI (i princip rapporten
till ECMWF).

13   Krieg, R., Andersson, C. (1986)
Vindmätningar i höga master, kvartals-
rapport 4/1985.

14   Dahlgren, L. (1986)
Solmätning vid SMHI.

15   Wern, L. (1986)
Spridningsberäkningar för ett kraftvärme-
verk i Sundbyberg.

16   Kindell, S. (1986)
Spridningsberäkningar för Uddevallas
fjärrvärmecentral i Hovhult.

17   Häggkvist, K., Persson, Ch., Robertson, L
(1986)
Spridningsberäkningar rörande gasutsläpp
från ett antal källor inom SSAB Luleå-
verken.

18   Krieg, R., Wern, L. (1986)
En klimatstudie för Arlanda stad.

19   Vedin, H. (1986)
Extrem arealnederbörd i Sverige.

20   Wern, L. (1986)
Spridningsberäkningar för lösningsmedel i
Tibro.

21   Krieg, R., Andersson, C. (1986)
Vindmätningar i höga master - kvartals-
rapport 1/1986.

22 Kvick, T. (1986)
Beräkning av vindenergitillgången på
några platser i Halland och Bohuslän.

23 Krieg, R., Andersson, C. (1986)
Vindmätningar i höga master - kvartals-
rapport 2/1986.

24 Persson, Ch. (SMHI), Rodhe, H.
(MISU), De Geer, L.-E. (FOA) (1986)
Tjernobylolyckan - En meteorologisk
analys av hur radioaktivitet spreds till
Sverige.

25 Fredriksson, U. (1986)
Spridningsberäkningar för Spendrups
bryggeri, Grängesberg.

26 Krieg, R. (1986)
Beräkningar av vindenergitillgången på
några platser i Skåne.

27 Wern, L., Ring, S. (1986)
Spridningsberäkningar, SSAB.

28 Wern, L., Ring, S. (1986)
Spridningsberäkningar för ny ugn,
SSAB II.

29 Wern, L. (1986)
Spridningsberäkningar för Volvo
Hallsbergverken.

30 Fredriksson, U. (1986)
SO_2-halter från Hammarbyverket kring ny
arena vid Johanneshov.

31 Persson, Ch., Robertson, L., Häggkvist, K.
(1986)
Spridningsberäkningar, SSAB - Luleå-
verken.

32 Kindell, S., Ring, S. (1986)
Spridningsberäkningar för SAABs
planerade bilfabrik i Malmö.

33 Wern, L. (1986)
Spridningsberäkningar för
svavelsyrafabrik i Falun.

34 Wern, L., Ring, S. (1986)
Spridningsberäkningar för Västhamns-
verket HKV1 i Helsingborg.

35 Persson, Ch., Wern, L. (1986)
Beräkningar av svaveldepositionen i
Stockholmsområdet.

36 Joelsson, R. (1986)
USAs månadsprognoser.

37 Vakant nr.

38 Krieg, R., Andersson, C. (1986)
Utemiljön vid Kvarnberget, Lysekil.

39 Häggkvist, K. (1986)
Spridningsberäkningar av freon 22 från
Ropstens värmepumpverk.

40 Fredriksson, U. (1986)
Vindklassificering av en plats på Hemsön.

41 Nilsson, S. (1986)
Utvärdering av sommarens (1986)
använda konvektionsprognoshjälpmedel.

42 Krieg, R., Kvick, T. (1986)
Vindmätningar i höga master.

43 Krieg, R., Fredriksson, U. (1986)
Vindarna över Sverige.

44 Robertson, L. (1986)
Spridningsberäkningar rörande gasutsläpp
vid ScanDust i Landskrona - bestämning
av cyanvätehalter.

45 Kvick, T., Krieg, R., Robertson, L. (1986)
Vindförhållandena i Sveriges kust- och
havsband, rapport nr 2.

46 Fredriksson, U. (1986)
Spridningsberäkningar för en planerad
panncentral vid Lindsdal utanför Kalmar.

47 Fredriksson, U. (1986)
Spridningsberäkningar för Volvo BMs
fabrik i Landskrona.

48 Fredriksson, U. (1986)
Spridningsberäkningar för ELMO-CALFs
fabrik i Svenljunga.

49 Häggkvist, K. (1986)
Spridningsberäkningar rörande gasutsläpp
från syrgas- och bensenupplag inom SSAB
Luleåverken.

50 Wern, L., Fredriksson, U., Ring, S. (1986)
Spridningsberäkningar för lösningsmedel i
Tidaholm.

51 Wern, L. (1986)
Spridningsberäkningar för Volvo BM ABs
anläggning i Braås.

52 Ericson, K. (1986)
Meteorological measurements performed
May 15, 1984, to June, 1984, by the
SMHI.

53 Wern, L., Fredriksson, U. (1986)
Spridningsberäkning för Kockums Plåt-
teknik, Ronneby.

54 Eriksson, B. (1986)
Frekvensanalys av timvisa temperatur-
observationer.

55 Wern, L., Kindell, S. (1986)
Luktberäkningar för AB ELMO i Flen.

56 Robertson, L. (1986)
Spridningsberäkningar rörande utsläpp av
NO_x inom Fagersta kommun.

57 Kindell, S. (1987)
Luften i Nässjö.

58 Persson, Ch., Robertson, L. (1987)
Spridningsberäkningar rörande gasutsläpp
vid ScanDust i Landskrona - bestämning
av cyanväte.

59 Bringfelt, B. (1987)
Receptorbaserad partikelmodell för
gatumiljömodell för en gata i Nyköping.

60 Robertson, L. (1987)
Spridningsberäkningar för Varbergs
kommun. Bestämning av halter av SO_2,
CO, NO_x samt några kolväten.

61 Vedin, H., Andersson, C. (1987)
E 66 - Linderödsåsen - klimatförhållanden.

62 Wern, L., Fredriksson, U. (1987)
Spridningsberäkningar för Kockums
Plåtteknik, Ronneby. 2.

63 Taesler, R., Andersson, C., Wallentin, C.,
Krieg, R. (1987)
Klimatkorrigering för energiförbrukningen
i ett eluppvärmt villaområde.

64 Fredriksson, U. (1987)
Spridningsberäkningar för AB Åetå-
Trycks planerade anläggning vid Kungens
Kurva.

65 Melgarejo, J. (1987)
Mesoskalig modellering vid SMHI.

66 Häggkvist, K. (1987)
Vindlaster på kordahus vid Alviks Strand -
numeriska beräkningar.

67 Persson, Ch. (1987)
Beräkning av lukt och föroreningshalter i
luft runt Neste Polyester i Nol.

68 Fredriksson, U., Krieg, R. (1987)
En överskalig klimatstudie för Tornby,
Linköping.

69 Häggkvist, K. (1987)
En numerisk modell för beräkning av
vertikal momentumtransport i områden
med stora råhetselement. Tillämpning på
ett energiskogsområde.

70 Lindström, Kjell (1987)
Weather and flying briefing aspects.

71 Häggkvist, K. (1987)
En numerisk modell för beräkning av
vertikal momentumtransport i områden
med stora råhetselement. En koefficient-
bestämning.

72 Liljas, E. (1988)
Förbättrad väderinformation i jordbruket -
behov och möjligheter (PROFARM).

73 Andersson, Tage (1988)
Isbildning på flygplan.

74 Andersson, Tage (1988)
Aeronautic wind shear and turbulence.
A review for forecasts.

75 Kållberg, P. (1988)
Parameterisering av diabatiska processer i
numeriska prognosmodeller.

76 Vedin, H., Eriksson, B. (1988)
Extrem arealnederbörd i Sverige
1881 - 1988.

77 Eriksson, B., Carlsson, B., Dahlström, B.
(1989)
Preliminär handledning för korrektion av
nederbördsmängder.

78 Liljas, E. (1989)
Torv-väder. Behovsanalys med avseende
på väderprognoser och produktion av
bränsletorv.

79 Hagmarker, A. (1991)
Satellitmeteorologi.

80 Lövblad, G., Persson, Ch. (1991)
Background report on air pollution
situation in the Baltic states - a
prefeasibility study.
IVL Publikation B 1038.

81 Alexandersson, H., Karlström, C.,
Larsson-McCann, S. (1991)
Temperaturen och nederbörden i Sverige
1961-90. Referensnormaler.

82 Vedin, H., Alexandersson, H., Persson, M. (1991)
Utnyttjande av persistens i temperatur och nederbörd för vårflödesprognoser.

83 Moberg, A. (1992)
Lufttemperaturen i Stockholm 1756 - 1990. Historik, inhomogeniteter och urbaniseringseffekt. Naturgeografiska Institutionen, Stockholms Universitet.

84 Josefsson, W. (1993)
Normalvärden för perioden 1961-90 av globalstrålning och solskenstid i Sverige.

85 Laurin, S., Alexandersson, H. (1994)
Några huvuddrag i det svenska temperatur-klimatet 1961 - 1990.

86 Fredriksson, U. och Ståhl, S. (1994)
En jämförelse mellan automatiska och manuella fältmätningar av temperatur och nederbörd.

87 Alexandersson, H., Eggertsson Karlström, C. och Laurin S. (1997).
Några huvuddrag i det svenska nederbördsklimatet 1961-1990.

88 Mattsson, J., Rummukainen, M. (1998)
Växthuseffekten och klimatet i Norden - en översikt.

89 Kindbom, K., Sjöberg, K., Munthe, J., Peterson, K. (IVL)
Persson, C. Roos, E., Bergström, R. (SMHI). (1998)
Nationell miljöövervakning av luft- och nederbördskemi 1996.

90 Foltescu, V.L., Häggmark, L (1998)
Jämförelse mellan observationer och fält med griddad klimatologisk information.

91 Hultgren, P., Dybbroe, A., Karlsson, K.-G. (1999)
SCANDIA – its accuracy in classifying LOW CLOUDS

92 Hyvarinen, O., Karlsson, K.-G., Dybbroe, A. (1999)
Investigations of NOAA AVHRR/3 1.6 μm imagery for snow, cloud and sunglint discrimination
(Nowcasting SAF)

93 Bennartz, R., Thoss, A., Dybbroe, A. and Michelson, D. B. (1999)
Precipitation Analysis from AMSU
(Nowcasting SAF)

94 Appelqvist, Peter och Anders Karlsson (1999)
Nationell emissionsdatabas för utsläpp till luft - Förstudie.

95 Persson, Ch., Robertson L. (SMHI) Thaning, L (LFOA). (2000)
Model for Simulation of Air and Ground Contamination Associated with Nuclear Weapons. An Emergency Preparedness Model.

96 Kindbom K., Svensson A., Sjöberg K., (IVL) Persson C., (SMHI) (2001)
Nationell miljöövervakning av luft- och nederbördskemi 1997, 1998 och 1999.

97 Diamandi, A., Dybbroe, A. (2001)
Nowcasting SAF
Validation of AVHRR cloud products.

98 Foltescu V. L., Persson Ch. (2001)
Beräkningar av moln- och dimdeposition i Sverigemodellen - Resultat för 1997 och 1998.

99 Alexandersson, H. och Eggertsson Karlström, C (2001)
Temperaturen och nederbörden i Sverige 1961-1990. Referensnormaler - utgåva 2.

100 Korpela, A., Dybbroe, A., Thoss, A. (2001)
Nowcasting SAF - Retrieving Cloud Top Temperature and Height in Semi-transparent and Fractional Cloudiness using AVHRR.

101 Josefsson, W. (1989)
Computed global radiation using interpolated, gridded cloudiness from the MESA-BETA analysis compared to measured global radiation.

102 Foltescu, V., Gidhagen, L., Omstedt, G. (2001)
Nomogram för uppskattning av halter av PM_{10} och NO_2

103 Omstedt, G., Gidhagen, L., Langner, J. (2002)
Spridning av förbränningsemissioner från småskalig biobränsleeldning
– analys av PM2.5 data från Lycksele med hjälp av två Gaussiska spridningsmodeller.

104 Alexandersson, H. (2002)
Temperatur och nederbörd i Sverige 1860 - 2001

105 Persson, Ch. (2002)
Kvaliteten hos nederbördskemiska mätdata
som utnyttjas för dataassimilation i
MATCH-Sverige modellen".

106 Mattsson, J., Karlsson, K-G. (2002)
CM-SAF cloud products feasibility study
in the inner Arctic region
Part I: Cloud mask studies during the 2001
Oden Arctic expedition

107 Kärner, O., Karlsson, K-G. (2003)
Climate Monitoring SAF - Cloud products
feasibility study in the inner Arctic region.
Part II: Evaluation of the variability in
radiation and cloud data

108 Persson, Ch., Magnusson, M. (2003)
Kvaliteten i uppmätta nederbördsmängder
inom svenska nederbörskemiska
stationsnät

109 Omstedt, G., Persson Ch., Skagerström, M
(2003)
Vedeldning i småhusområden

110 Alexandersson, H., Vedin, H. (2003)
Dimensionerande regn för mycket små
avrinningsområden

111 Alexandersson, H. (2003)
Korrektion av nederbörd enligt enkel
klimatologisk metodik

112 Joro, S., Dybbroe, A.(2004)
Nowcasting SAF – IOP
Validating the AVHRR Cloud Top
Temperature and Height product using
weather radar data
Visiting Scientist report

113 Persson, Ch., Ressner, E., Klein, T. (2004)
Nationell miljöövervakning – MATCH-
Sverige modellen
Metod- och resultatsammanställning för
åren 1999-2002 samt diskussion av
osäkerheter, trender och miljömål

114 Josefsson, W. (2004)
UV-radiation measured in Norrköping
1983-2003.

115 Martin, Judit, (2004)
Var tredje timme – Livet som
väderobservatör

116 Gidhagen, L., Johansson, C., Törnquist, L.
(2004)
NORDIC – A database for evaluation of
dispersion models on the local, urban and
regional scale

117 Langner, J., Bergström, R., Klein, T.,
Skagerström, M. (2004)
Nuläge och scenarier för inverkan på
marknära ozon av emissioner från Västra
Götalands län – Beräkningar för 1999

118 Trolez, M., Tetzlaff, A., Karlsson, K-G.
(2005)
CM-SAF Validating the Cloud Top Height
product using LIDAR data

119 Rummukainen, M. (2005)
Växthuseffekten

120 Omstedt, G. (2006)
Utvärdering av PM_{10} - mätningar i några
olika nordiska trafikmiljöer

121 Alexandersson, H. (2006)
Vindstatistik för Sverige 1961-2004

SMHI